Aptamer conjugated Si nanowire network/poly(pyrrole)-NTA structure for electrochemical sensing

Monica Vallejo-Perez, Essohanam Beke, Chantal Gondran, Karine Gorgy, Isabelle Gélard, Céline Ternon, Nicolas Spinelli, Valérie Stambouli

Sensing and Bio-Sensing Research 42 (2023) 100593

Contents lists available at ScienceDirect

Sensing and Bio-Sensing Research

journal homepage: www.elsevier.com/locate/sbsr

Aptamer conjugated Si nanowire network/poly(pyrrole)-NTA structure for electrochemical sensing

Monica Vallejo-Perez [a,b], Essohanam Beke [b], Chantal Gondran [b,*], Karine Gorgy [b], Isabelle Gélard [a], Céline Ternon [a], Nicolas Spinelli [b], Valérie Stambouli [a,*]

[a] Univ. Grenoble Alpes, CNRS, Grenoble INP, LMGP, F-38000 Grenoble, France
[b] Univ. Grenoble Alpes, CNRS, DCM UMR 5250, F. 38000 Grenoble, France

ARTICLE INFO

Keywords:
Si nanonet
TBA aptamer
Thrombin
Electrochemical impedance spectroscopy
Cyclic voltammetry

ABSTRACT

The current study describes the design, analytical characterization, and testing of aptamer sensors based on Si nanonets (Si NN) for thrombin electrochemical detection. Si nanonets are thin sheet arrays of randomly aligned Si nanowires with controlled and programmable properties that may be transported and integrated on a variety of substrates. Si nanonets were placed onto a commercial glassy carbon working electrode to create our aptasensor. Then they were functionalized by conductive pyrrole polymerization, which was followed by aptamer bioreceptor grafting. Electrochemical detection of thrombin was carried out after optimizing the electrode properties. On the one hand, cyclic voltammetry analyses demonstrated a linear association between the acquired current and the logarithm of thrombin concentration from 5 nmol L^{-1} to 2 μmol L^{-1}. Impedance measurements, on the other hand, revealed a linear relationship between the charge transfer resistance as well as the impedance modulus. Thus, for the first time, Si nanonet thin sheets were used as constitutive nanoporous parts of electrodes capable of detecting thrombin at concentration limits of 5 nM, considered as a risk factor or presence of thrombosis. This demonstrates the concept of using this type of nanomaterial to detect molecules of biological interest.

1. Introduction

Sensor platforms with aptamers as capture molecules -also called aptasensors- more and more often involve nanostructured materials in view of sensitive and specific target molecule detection and quantification. Indeed, combining the strategic properties of both aptamers and nanomaterials opens the way to enhancing detection performances. On the one hand, aptamers are synthetic short single-stranded ssDNA (or RNA) oligonucleotides characterized by a 3D conformation specifically suited to bind with high affinity a target analyte which can be cells [1,2], small molecules [3] or macromolecules such as proteins [4]. As an alternative to antibodies, aptamers exhibit many advantages, which are extensively described in the reviews of both K. Urmann [5] and H. Yoo [6]. Among their advantages, they are less affected by temperature fluctuations, they are more stable and they offer versatile chemical modification options that facilitate their surface conjugation in a desired orientation and density. On the other hand, detection platforms based on highly developed surface nanostructured material benefit from improved detection performance. Different kinds of nanomaterials are employed depending on the detection method. Among the various detection methods, electrochemical detection, specifically electrochemical impedance spectroscopy (EIS), is well-suited for point-of-care (PoC) detection applications as it avoids the need for additional labelling and time-consuming processes [7,8]. In this case, nanomaterials with specific electrical characteristics are required. Carbon nanotubes (CNT) [7,9,10], and later graphene [11] are commonly used as candidates because of their beneficial electronic and optical properties for enhanced signal capture of biological recognition events. Nanostructured metals such as Au on flexible substrates are also employed notably for thrombin detection with very good sensing performances [12]. More recently, nanostructures of transition metal dichalcogenide such as MoS_2 [13] and WS_2 [14], exhibiting thin layers of nanosheets have shown their appropriateness in electrochemical biosensor setups for biodetection. However, they did not provide superior properties

* Corresponding authors.
E-mail addresses: Essohanam.Beke@univ-grenoble-alpes.fr (E. Beke), chantal.gondran@univ-grenoble-alpes.fr (C. Gondran), karine.gorgy@univ-grenoble-alpes.fr (K. Gorgy), isabelle.gelard@grenoble-inp.fr (I. Gélard), celine.ternon@grenoble-inp.fr (C. Ternon), Nicolas.Spinelli@univ-grenoble-alpes.fr (N. Spinelli), valerie.stambouli-sene@grenoble-inp.fr (V. Stambouli).

https://doi.org/10.1016/j.sbsr.2023.100593
Received 12 July 2023; Received in revised form 6 October 2023; Accepted 17 October 2023
Available online 18 October 2023

compared to the other described nanomaterials for electrochemical biosensing applications. Alternatively, as a classical and standard semiconducting material used in microelectronics, Si and its nanostructured counterparts, silicon nanowires (Si NWs), with their perfectly tunable electrical and shape characteristics [15,16], are promising candidates for aptamer conjugation and/grafting [5,17]. This can be performed *via* the creation of hybrid inorganic/organic nanocomposite materials such as polymer-modified Si NWs. For instance, vertical Si NW arrays were modified with glycopolymer for TD05 aptamer grafting in view of cancer cell detection using fluorescence [1]. Alternatively, to these vertical Si NW arrays, another more confidential shape of Si NW arrays involves Si nanonets (Si NNs) [18]. These combine numerous advantages such as the network benefits from the good intrinsic properties of each individual Si NW or the excellent reproducibility of fabrication (easy and low cost) due to control of NW density. Moreover, their electrochemical properties are reproducible; they are flexible and non-toxic [18]. Similarly to CNT thin layer shapes [19], these nanonets are scalable arrays of randomly oriented Si NWs, that can be transferred and integrated on a wide range of substrates [18]. Our group has previously reported the fabrication of Si NNs [20], their transfer and integration in Field effect Transistors (FETs) devices to build Si NNFETs [21]. More recently, as a seminal study for their use for biodetection, the influence of the grafting of a model bioreceptor (Thrombin Binding Aptamer, TBA–15) on the semiconducting characteristic variations of such devices was carefully studied in view of thrombin recognition [22].

So far, such Si NN thin layers have not yet been tested as a working electrode (WE) constitutive material, involving TBA-15 bioreceptor grafting in view of electrochemical detection of thrombin. Few reports in the literature rely on electrochemical sensors based on Si NWs, most of which are built from 3D vertically oriented Si nanowire-based structures [23–35]. To our knowledge, only two electrochemical biosensors based on Si NN thin layers have been reported so far [36,37]. In both cases, they were voltammetric sensors. In the first study [36], a Pt electrode served as the WE onto which glucose oxidase enzyme-modified Si NNs were transferred to construct a glucose sensor. In the second one [37], in view of DNA detection, Si NN decorated with gold nanoparticles, in order to increase the performance of the biosensor were transferred onto the ITO electrode.

In this context, we report the construction of an aptasensor on a glassy carbon (GC) electrode, using the biotin-labeled TBA-15 bioreceptor for thrombin detection on an Si NN based architecture. We particularly investigated step by step the elaboration of our aptasensor using characterization techniques such as SEM to visualize the surface morphology, cyclic voltammetry (CV) and electrochemical impedance spectroscopy (EIS) as architecture characterization methods. Then, after optimizing some characteristics of our aptasensor mainly in terms of Si NN density, the performance of our aptasensor toward thrombin target detection was assessed by CV and EIS.

2. Materials and methods

2.1. Chemicals

TBA–15 $^{5'}$GGT TGG TGT GGT TGG TTT TTT$^{3'}$–biotin was synthesized at DCM (département de chimie moléculaire, France) on a DNA synthesizer (ABI 3400, Foster city, CA, USA) using the phosphoramidite protocol. Thrombin: freeze-dried human α-thrombin molecules were obtained from Merck (L'isle d'Abeau, France). Lysozyme, human IgG, BSA, $FeCl_3$, $K_3Fe(CN)_6$, $K_4Fe(CN)_6$, and $CuCl_2$ were obtained from Aldrich (L'isle d'Abeau, France). They were used as received without further purification.

2.2. Instrumentation and characterization

SEM images of the different electrodes modified by the polymer were carried out using a ZEISS Gemini 300 field-emission scanning electron microscopy (FESEM) instrument (Carl Zeiss, Oberkochen, Germany) with an accelerating voltage of 3 and 5 kV.

Electrochemical properties were investigated by using a conventional three-electrode potentiostat coupled to a PGSTAT 100 (Eco Chemie, Utrecht, The Netherlands, Metrohm AG). The working electrode (Biologic, France) was a glassy carbon (GC) electrode (diameter 3 mm) thoroughly cleaned using 20 μm diamond paste and rinsed with acetone, ethanol, and distilled water before use. A saturated calomel electrode (SCE) (Hach-Lange, Germany) was used as a reference electrode, while a wire of Pt was used as a counter electrode (Métaux précieux de France, France). All the cyclic voltammetry (CV) and electrochemical impedance spectroscopy (EIS) measurements were carried out at 25 °C by using the mixture $[Fe(CN)_6]^{3-/4-}$ (2 mmol L^{-1}) as a redox probe in phosphate buffer (0.1 mol L^{-1}, pH = 7) unless specified. CV measurements were performed using Nova 2.1.2 and 2.1.4 software, whereas EIS measurements were achieved with FRA software. The frequency sweep to perform EIS experiments was chosen from 50 kHz to 0.01 Hz at a fixed potential of 0.18 V/SCE with an AC amplitude of 10 mV_{rms}. The potential of 0.18 V was selected since it corresponds to the equilibrium potential of the $[Fe(CN)_6]^{3-/4-}$ redox couple. Zview (Scribner Associates Inc.) software was used to simulate the data.

2.3. Fabrication of Si nanonet aptasensors and thrombin detection

The schematic illustration in Fig. 1 presents the main construction steps of the aptasensor involving a nanocomposite architecture. The latter is constituted of Si NN, functionalized polypyrrole and complexed Cu^{2+}. Specifically, it results from the chemical polymerization of a pyrrole monomer, which is functionalized by a nitrilo-triacetic acid (NTA) termination **1** (Fig. 1a and b) on the Si NN. Through the (NTA) termination, the Cu^{2+} complexation on the polymer is performed, enabling the subsequent grafting of biotin-labeled TBA-15 bioreceptor [38] **2** (Fig. 1 c and d) and the thrombin target recognition (Fig. 1 e). Each of these steps are detailed in the following.

2.3.1. Si NN fabrication

The Si NN elaboration was previously described by our group [20–22]. Briefly, the process starts with a suspension of Si nanowires, which were previously grown by vapor-liquid-solid (VLS) deposition [40] controlling both NWs diameter and crystallinity [41]. The Si NWs have an average diameter of 39 ± 7 nm, an average length of 7 ± 3 μm and present a low-doped p-type semiconductor behavior (doping level of about 10^{16} atom cm^{-3}). The Si NWs concentration was controlled in solution by absorption spectroscopy at 400 nm. The Si nanonet assembly was obtained by vacuum filtration through a nitrocellulose membrane. The surface density of the nanonet (NWs cm^{-2}) is directly related to the filtered volume of suspension [20]. In this work, several surface densities were explored, which correspond to surface coverage of 15, 54 and 100%. Herein, the nitrocellulose membrane supporting the Si nanonet was immersed in a dichlorobenzene solution for 30 s in order to remove the air within the pores and achieve good adherence between the substrate and the Si nanonet. Then, the nanonet was transferred to the glassy carbon electrode (Fig. 1a), which has been previously cleaned as detailed in part 2.2. The assembly was left in air for 4 min. Finally, the nitrocellulose membrane was dissolved in an acetone bath for 35 min, leaving the electrode with the Si nanonet on top. It was then cleaned in acetone and isopropanol and dried under nitrogen gas flow.

2.3.2. PPY-NTA film deposition

Pyrrole-NTA monomer was synthesized as described previously [42]. The PPy-NTA deposition on the GC/Si nanonet electrode was obtained by monomer adsorption in liquid conditions, followed by chemical oxidative polymerization in the presence of $FeCl_3$ [43,44]. The developed step-by-step process is the following:

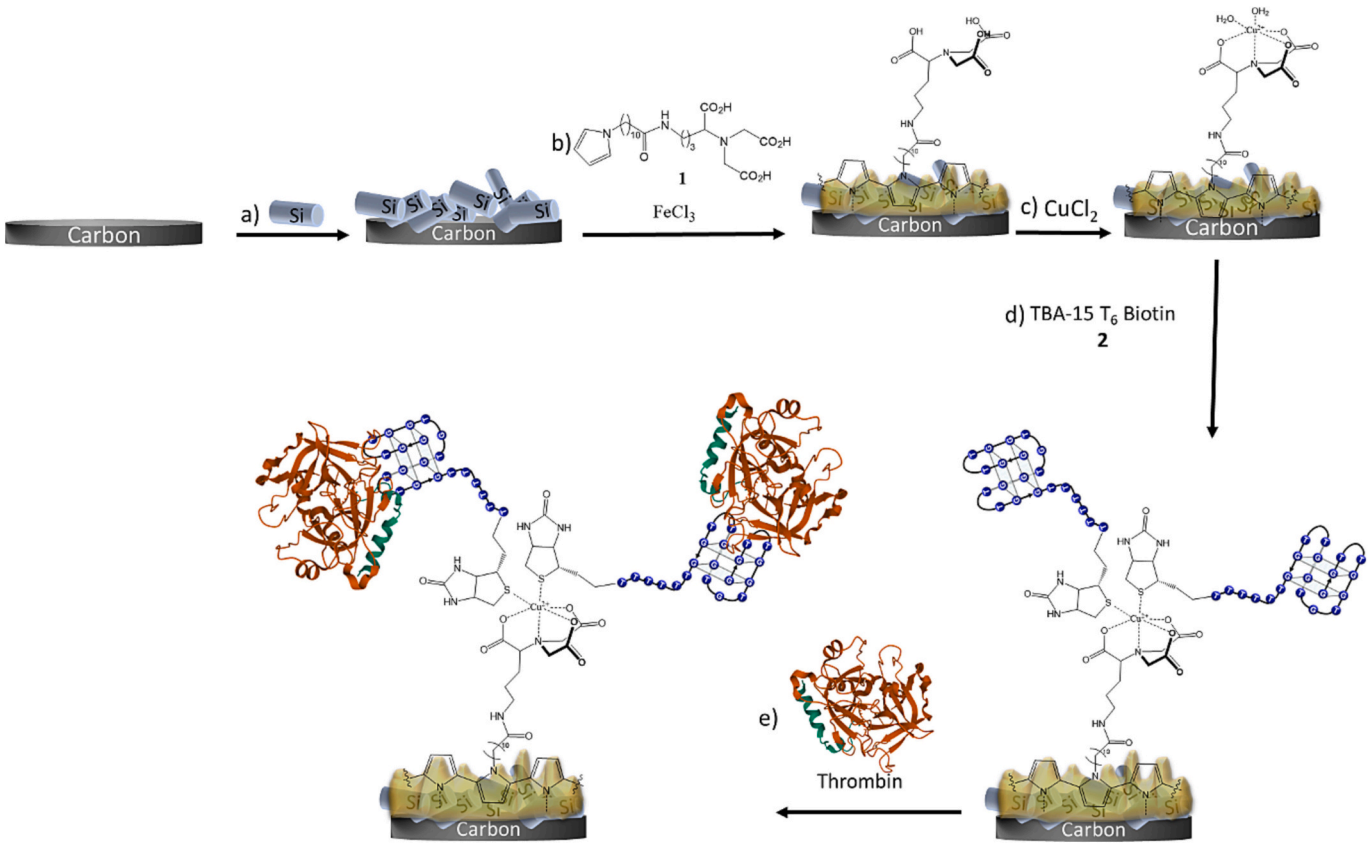

Fig. 1. sketch of the elaboration of the aptamer sensor on glassy carbon electrode; (a) transfer of Si nanonet (Si NN), (b) pyrrole –NTA polymerization, (c) Cu^{2+} complexation, (d) TBA immobilization, (e) recognition of thrombin. Structure of thrombin is based on pdb 3U8T [39].

(i) GC/Si nanonet electrode preparation: The electrode was subjected to vacuum pumping at 40 °C for 30 min. The aim of this process was to eliminate possible solvent residues that could remain in the nanonet after the transfer process and to improve the adherence between the carbon surface and the Si nanonet.

(ii) Surface activation of the GC/Si NN based electrode: The GC/Si NN electrode was exposed to a UV-ozone treatment for 10 min to activate the surface of the electrode, leading to the formation of hydroxyls (OH), carbonyl (C=O) or carboxylic acids (C(=O)OH) groups on its surface [45].

(iii) Pyrrole-NTA monomer adsorption in liquid conditions: The GC/Si NN electrode was immersed for 1 h in 100 μL of a 5 mmol L^{-1} solution of pyrrole-NTA in acetonitrile (C_2H_3N), which was acidified by the addition of perchloric acid ($HClO_4$) to enable the solubilization of the monomer (Fig. 1b). After 1 h of exposure to pyrrole-NTA solution, the electrode was carefully washed for 10 min and under stirring (150 rpm), in a phosphate buffer solution (0.1 mol L^{-1}, pH 7) to remove the excess pyrrole that was not adsorbed on the electrode surface.

(iv) Polypyrrole-NTA chemical oxidative polymerization: The electrode was exposed for 1 h to $FeCl_3$ (0.1 mol L^{-1}) in HCl (0.1 mol L^{-1}) solution. Subsequently, in order to remove the sections of the polymer film that were not properly attached to the surface, the electrode was rinsed overnight under stirring (150 rpm) in a phosphate buffer solution (pH 7).

2.3.3. Cu^{2+} complexation

The PPy-NTA modified GC/Si nanonet electrode was immersed for 20 min in a 0.01 mol L^{-1} copper chloride ($CuCl_2$) solution in acetate buffer (0.1 mol L^{-1}) at pH 4.8 to obtain the Cu^{2+} complexation on the NTA (Fig. 1c). The electrode was then subjected to different rinsing processes under stirring (150 rpm), first in a 0.5 mol L^{-1} sodium chloride (NaCl) solution for 5 min, followed by a rinsing in a phosphate buffer solution at pH 7 for 5 min.

2.3.4. Bioreceptor immobilization (Fig. 1d)

This was carried out by exposing the GC/Si nanonet/Cu^{2+} electrode to 100 μL of 50 μM TBA-15 solution in phosphate buffer at pH 7 for 45 min. Before use, the TBA-15 solution was heated at 90 °C for 3 min, and cooled by immersion into an ice bath to obtain a proper folding structure [8]. Subsequently, the electrode was rinsed for 10 min (under stirring at 150 rpm) in a phosphate buffer solution at pH 7 to remove the TBA-15 bioreceptors that were not properly grafted to the electrode surface.

2.3.5. Thrombin recognition

The Si NN based electrochemical biosensor was exposed to 100 μL of a given concentration of thrombin (Fig. 1e) in phosphate buffer (0.1 mol L^{-1}, pH 7.4) containing 0.01 mol L^{-1} of NaCl, 5 mmol L^{-1} of KCl and 1 mmol L^{-1} of $MgCl_2$ for 30 min. Subsequently, the electrode was rinsed under stirring (150 rpm) in phosphate buffer (pH 7) for 10 min.

3. Results and discussion

3.1. Construction and characterization of the Si NN-based aptasensor

3.1.1. Si NN deposition on the GC electrode surface

The first experiments consisted of characterizing the role played by the Si NN on top of the GC electrode. For that, the Si NN density approximates 468 × 10^6 NWs cm^{-2}, which means Si NN surrounds the whole electrode surface (100% covered). These thin layers of Si NN transferred on GC were studied by CV and EIS, with $[Fe(CN)_6]^{3-/4-}$ as redox probe. A peak current decrease and impedance increase were obtained (data not shown). It appeared that the semi-conducting properties of Si NNs were not adapted under these conditions to exalt the

surface of the electrode. Indeed, in the range of potential used, the layer of Si NNs is not sufficiently conductive to enhance the electron transfer of the redox probe. So, Si NNs are only used as a scaffold for the thrombin recognition layer. In order to promote electron transfer while increasing the recognition layer, Si NNs with lower densities were used. Si NN with a density equivalent to 199×10^6 NWs cm^{-2} corresponding to a surface coverage of about 54% can be observed on SEM images (Fig. 2 a, b) where the glassy carbon surface seems accessible.

3.1.2. Chemical polymerization of Pyrrole-NTA

The technique consisted of the deposition of a poly(11-pyrrol-1-yl-undecanoicacid N_α',N_α-bis(carboxymethyl)-L-lysine amide) film (PPy-NTA) on the Si NN (Fig. 1 b). Generally, the deposition of polypyrrole films on highly conductive electrodes is performed by *in situ* electropolymerization of the monomer, through the electrochemical activation of the pyrrole group in order to carry out its polymerization by oxidative electrolysis [38]. In our case, this technique was not efficient for generating a polymer film since the Si NNs covering the GC electrode were not conductive enough. Additionally, they were covered by a SiO_2 native oxide layer, which reduces the electric conduction between the Si NWs. Consequently, we explored the possibility of carrying out a chemical deposition of the PPy-NTA film on the GC/Si NN-based electrodes. Indeed, several studies have shown that pyrrole polymerization can be chemically carried out on various substrates (glass, SiO_2, carbon) [46–49].

More particularly, here the objective was to develop a technique that allowed depositing a PPy-NTA film covering the entire surface of the electrode, *i.e.*, both the Si NN and the naked carbon surface. In addition, it was essential that the deposited film fit the nanonet structure, and it should be thin enough to preserve the porous shape of the electrode provided by the addition of Si NN. For these reasons, the PPy-NTA film chemical deposition process was studied on GC electrodes covered by a Si NN with a density equivalent to 199×10^6 NWs cm^{-2} corresponding to a surface coverage of about 54% as observed on the SEM images (Fig. 2 a, b).

The changes in the morphology and microstructure of the electrode after the PPy-NTA polymerization process on GC/Si NN were clearly observed when comparing the SEM images obtained before (Fig. 2 a, b) and after polymerization (Fig. 2 c, d). The polymer film fits the morphology of the nanonet, keeping the high-specific surface, which will lead to a higher amount of bioreceptors that could be grafted onto the surface in the subsequent stages.

To analyze the PPy-NTA chemical deposition process on the GC/Si NN based electrode, the electrochemical properties were studied by cyclic voltammetry (Fig. 3A) and EIS (Fig. 3B), in the presence of the $[Fe(CN)_6]^{3-/4-}$ redox probe, before and after PPy-NTA chemical deposition. Nyquist plots exhibit a significant increase in the radius of the semicircle once the polymerization process is performed (Fig. 3A(b)) confirming the blocking effect of electron transfer on the redox probe caused by PPy-NTA film deposition. Besides, the standard Randles equivalent circuit obtained by data fitting helped to elucidate the phenomena occurring on the electrode after the PPy-NTA deposition (Table 1). The Randles circuit consists of an electrolyte resistance in series with the parallel combination of the double-layer capacitance C_{dl} and a resistance of a faradic reaction composed of a charge tranfer resistance R_{CT} and a Warburg impedance.

We replaced the capacities with constant phase elements (CPE) in order to take into account the inhomogeneity that is commonly associated with modified electrodes with a high roughness factor [50,51]. A good match between the experimental points and the fitting curve can be observed in Fig. 3B where the line through the data points represents the fitting curve using this equivalent circuit. First, as expected, the blocking effect of electron transfer on the redox probe was confirmed by the increase of the charge transfer resistance, R_{ct}, from 1220 to 5800 Ω

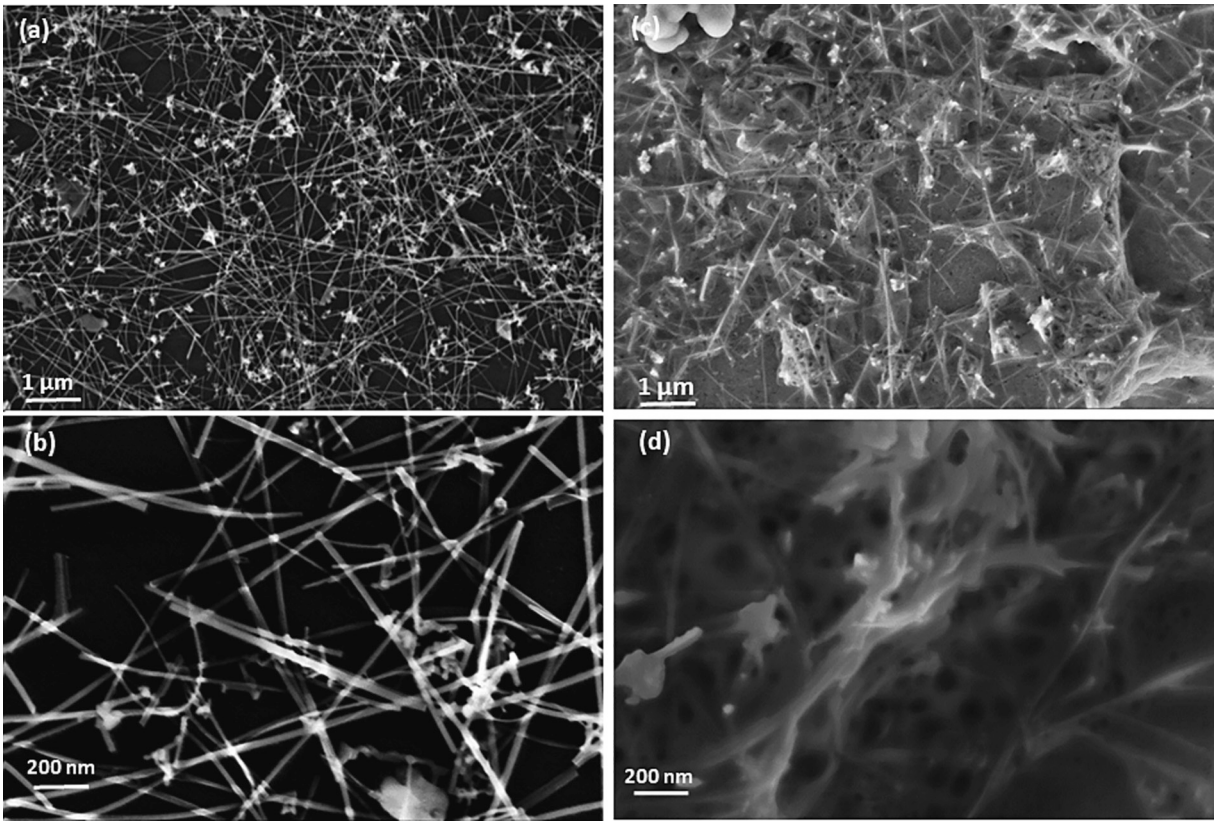

Fig. 2. SEM images of GC/Si NN based electrode: (a) and (b) before polypyrrole-NTA deposition, (c) and (d) after polypyrrole-NTA modification (Si NN surface coverage of 54%).

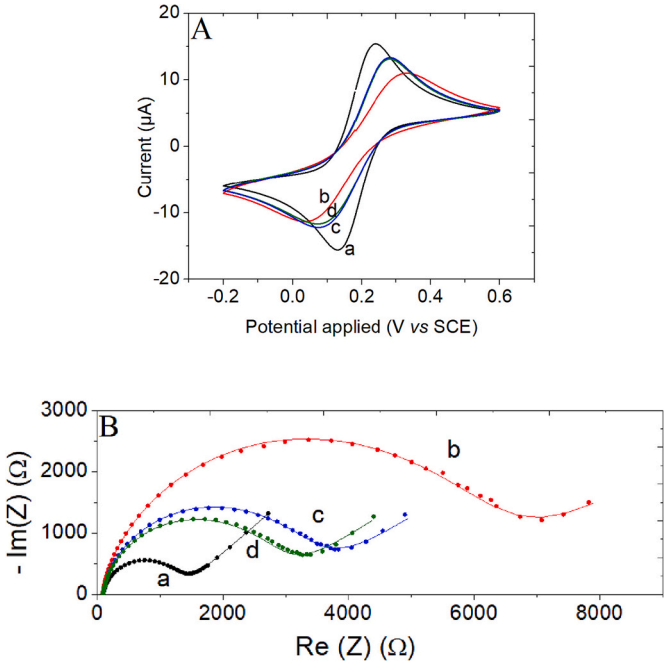

Fig. 3. Electrochemical characterization of a GC/Si NN based electrode (a) before; (b) after the deposition of the polypyrrole-NTA film; (c) after copper complexation (GC/Si NN/PPy-NTA/Cu^{2+}) and (d) after TBA-15 grafting as indicated in each figure: (A) Cyclic voltammogram recorded at scan rate of 10 mV/s, and (B) Nyquist plot of impedance spectra obtained at OCP, with an amplitude alternative potential of 10 mV_{RMS} and a frequency sweep from 50,000 Hz to 0.1 Hz. Dots represent the experimental data and lines represent the fitted data. All measurements performed using 2 mmol L^{-1} $[Fe(CN)_6]^{3-/4-}$ redox probe in 0.1 mol L^{-1} phosphate buffer (pH 7 at 25 °C).

Table 1
Values of the equivalent circuit elements: charge transfer resistance, R_{ct}, double layer capacitance, C_{dl}, and characteristic frequency, f, obtained by data fitting for a GC/Si NN based electrode (Si NN surface density of 54%), after deposition of the PPy-NTA film (GC/Si NN/PPy-NTA), after copper complexation (GC/Si NN/PPy-NTA/Cu^{2+}) and after TBA-15 grafting (GC/Si NN/PPy-NTA/Cu^{2+}/50 μM TBA-15).

Step	R_{ct} (Ω)	C_{dl} (μF)*	f (Hz)
GC/Si NN	1220 ± 20	1.89 ± 0.03	69.2
GC/Si NN/PPy-NTA	5800 ± 90	2.58 ± 0.04	10.6
GC/Si NN/PPy-NTA/Cu^{2+}	3170 ± 50	2.16 ± 0.03	23.3
GC/Si NN/PPy-NTA/ Cu^{2+}/50 μM TBA-15	2660 ± 40	2.13 ± 0.03	28.2

* C_{dl} is calculated from the value of the CPE.

upon deposition of PPy-NTA film. Concerning the double layer capacitance, C_{dl}, it increased after the polymer deposition step (from 1.89 to 2.58 μF). Finally, regarding the characteristic frequency, f, as expected, an important decrease in this parameter was observed after the surface modification by the polymer film. Thus, the electron transfer is slowed down at the electrode surface once the PPy-NTA film is deposited due to the low permeability of the latter.

3.1.3. Cu^{2+} complexation

Nitrilotriacetic acid (NTA) chelates metal ions such as Cu^{2+} or Ni^{2+} [38,52–56]. The copper ion was chosen for the construction of the modified electrode architecture for the detection of thrombin (Fig. 1, c). Complexation was performed by dipping the electrode into a $CuCl_2$ solution.

The electrochemical properties of the modified electrode change significantly after this step. The CV spectra (Fig. 3A (c)) show an increase in the intensity of both current peaks (43% for I_{pa} and 29% for I_{pc}), as well as a decrease of ΔE_p, meaning that the electron transfer is faster after the Cu^{2+} complexation step. It is probably due to an electrostatic attraction between the positive charges brought by the Cu^{2+} and the negative charges of the redox probe ($[Fe(CN)_6]^{3-/4-}$) thus facilitating the passage of the latter through the 3D structure toward the conductive surface of the electrode.

This result is coherent with the one obtained by EIS and data fitting (Fig. 3B (c), Table 1). An important decrease in the radius of the semicircle and in the charge transfer resistance (from 5800 to 3170 Ω) after the Cu^{2+} complexation step is observed. With regard to the other parameters studied, it can be noted that the double layer capacitance decreased after the metallic complexation step (from 2.58 to 2.16 μF). It can be assumed that the charges added by Cu^{2+} ions in the polymer have modified the structure of the double layer, which could lead to the evolution of its thickness. Finally, the evolution of the characteristic frequency showed that, as expected, the electron transfer is accelerated once Cu^{2+} was present in the polymer. The increase of f seems to indicate that the permeability of the polymer film is improved by the presence of Cu^{2+}, which facilitates the passage of redox probes. This is certainly linked to better hydration of the polymer.

3.1.4. TBA-15 aptamer immobilization

The immobilization of the bioreceptor on the polymer film can be carried out by affinity interactions between chelated copper and bioreceptors carrying either a polyhistidine or a biotin moiety, according to the literature [38,57]. We used this property to immobilize the biotinylated TBA-15 bioreceptor (Fig. 1d). Regarding the TBA-15 concentration, two concentrations were tested, *i.e.* 10 and 50 μmol L^{-1}. As a result, the choice was made to use 50 μmol L^{-1} as it provides better detection.

At this step, it would be expected to see a decrease in current peaks and an increase in impedance due to the steric effect inducted by the grafted bioreceptor (TBA-15). The opposite result was observed since there was a significant decrease in the radius of the semicircle (Fig. 3B (d)), as well as in R_{ct} (from 3170 to 2660 Ω) (see Table 1). This analysis was carried out on 6 different biofunctionalized Si nanonet-based electrodes. In all cases a decrease in impedance was observed after the TBA-15 immobilization step. Moreover, the electrochemical properties of the biofunctionalized Si nanonet-based electrodes remained stable during 24 h. On the other hand, C_{dl} was not significantly modified, while only the frequency characteristic increased significantly from 23.3 to 28.2 Hz. The acceleration of the electron transfer observed through the decrease in R_{ct} and the increase in f seems to indicate that some PPy-NTA oligomers have come off the polymer film during the functionalization step by the TBA-15. An hypothesis that could explain the stability of the C_{dl} after the bioreceptor grafting step would be that the detached oligomers were not contained in the parts of the film supporting the electrochemical double layer. The cyclic voltammetry technique was not sufficiently sensitive to detect this change (Fig. 3A (d)).

3.1.5. Effect of the Si nanonet density

Regarding the effect of Si nanonet density, in the presence of the redox probe, the CV and the EIS were compared for three GC/Si NN/PPy-NTA/Cu^{2+}/50 μmol L^{-1} TBA-15 modified electrodes with varying densities (0, 15, 54%) of Si NN (Fig. 4). Moreover, a bare GC electrode (without any modification) was tested as a reference. Here, it is important to mention that the adsorption time of the PPy-NTA monomer and the temperature remained constant in all the studied cases during the fabrication step. Thus, it can be assumed that the amount of PPy-NTA film formed is similar in quantity of PPy-NTA units for each of the electrodes studied.

As expected, the best electrochemical activity was observed on the bare electrode. This was evidenced by the higher values of the peak currents (I_{pa} and I_{pc}) in the CV (Fig. 4A (a), Table 2) and the smaller radius of the semicircle, together with the lower value of the charge transfer resistance for the EIS analyses (Fig. 4B (a), Table 2).

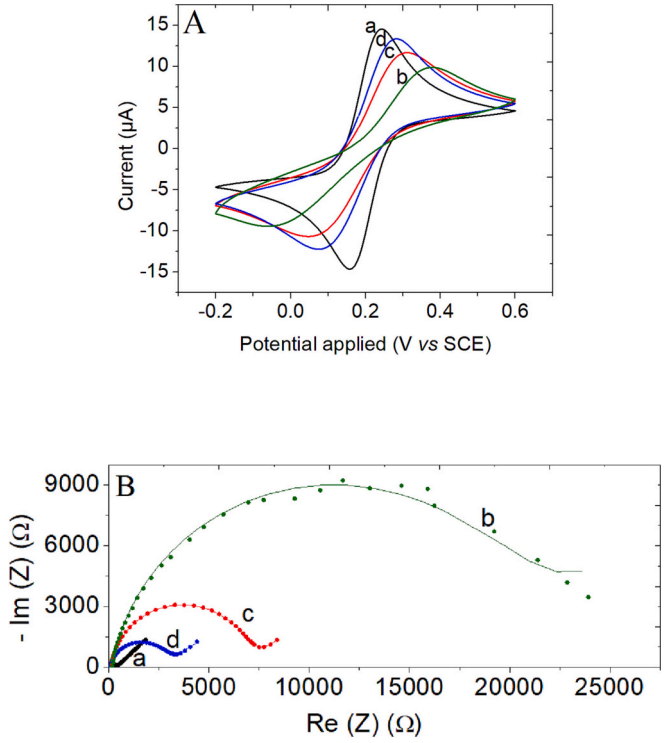

Fig. 4. Electrochemical characterization of bare GC electrode (a) and of GC/Si NN/PPy-NTA/Cu^{2+}/50 μM TBA-15 modified electrodes with NN densities of (b) 0, (c) 15 (d) 54% as indicated in each figure: (A) Cyclic voltammogram recorded at scan rate of 10 mV/s, and (B) Nyquist plot of impedance spectra obtained at OCP, with an amplitude alternative potential of 10 mV_{RMS} and a frequency sweep from 50,000 Hz to 0.1 Hz. Dots represent the experimental data and lines represent the fitted data. All measurements performed using 2 mmol L^{-1} $[Fe(CN)_6]^{3-/4-}$ redox probe in 0.1 mol L^{-1} phosphate buffer (pH 7), at 25 °C.

Table 2
Values of the different parameters investigated by cyclic voltammetry and electrochemical impedance spectroscopy (values of the equivalent circuit elements obtained by data fitting) on the 4 electrodes detailed in Fig. 4.

	I_{pa} (μA)	I_{pc} (μA)	ΔE_p (V)	R_{ct} (Ω)	C_{dl}* (μF)	f (Hz)
GC	14.5	−14.6	0.087	298 ± 6	0.90 ± 0.02	590
GC/54% Si NN/ PPy-NTA/Cu^{2+} /50 μM TBA-15	13.8	−12.9	0.170	2660 ± 40	2.13 ± 0.03	28.2
GC/15% Si NN/ PPy-NTA/Cu^{2+} /50 μM TBA-15	11.6	−10.7	0.266	6800 ± 100	1.8 ± 0.3	13.3
GC/PPy-NTA/Cu^{2+} /50 μM TBA-15	9.9	−9.4	0.449	20,300 ± 300	3.7 ± 0.5	2.1

* C_{dl} is calculated from the value of the CPE.

For the electrode on which solely a PPy-NTA film was deposited (GC/PPy-NTA/Cu^{2+}/50 μM TBA-15) corresponding to 0% of Si NN surface coverage, poor electrochemical activity was shown as evidenced by the low peak currents as well as the large value of ΔEp, indicating an important decrease in the reversibility of the electrochemical reaction (Fig. 4A (b) and Table 2). Likewise, the EIS analysis showed a strong increase in the impedance of the system (Fig. 4B (b), Table 2), where the charge transfer resistance increased by 9 times and the characteristic frequency decreased by 280 times with respect to the carbon electrode without any surface modification. We can also observe a strong modification of C_{dl} which is multiplied by 4. The origin of these results can be traced to the formation of a dense, compact, and continuous polypyrrole film on the electrode surface, preventing proper ion exchange between the solution and the conductive surface of the electrode. The modified electrodes where the Si NNs were present exhibit an intermediate behavior. As can be seen in CV graphs (Fig. 4A (c,d) and Table 2), a lower density of Si NNs results in a less accessible electrode surface for the redox probe. The lower peaks evidence this: 11.6 μA compared to 13.8 μA for I_{pa}, and − 10.7 μM compared to −12.9 μA for I_{pc} (with 15% and 54% Si NN surface coverage, respectively). This result is confirmed from EIS diagrams (Fig. 4A (c,d) and Table 2) by the high value of the charge transfer resistance obtained in the case of the less dense Si NNs (6800 Ω for 15% Si NN surface coverage) compared to the value obtained in the case of the denser Si NNs (2660 Ω for 54% Si NN surface coverage). Besides, the better permeability generated by the modification of the carbon electrode with Si NNs was reflected in the results obtained for the three following parameters: R_{ct}, C_{dl} and f. As shown in Table 2, when the Si NN structure is present, these three parameters were closer to those obtained for the bare carbon electrode, than those obtained for the electrode modified only by the PPy-NTA film (without Si NN). Thus, the presence of the Si NN allowed the modified electrode to maintain a good electrochemical response.

These results allowed us to conclude that the backbone formed by the Si NNs induced structuration of the obtained thrombin recognition film, instead of having a thick, compact and continuous layer. Thus, the denser the Si NNs, the more structured the recognition film, allowing the redox probe to have easier access to the underlying carbon electrode. Consequently, the denser Si NN based electrode (54% Si NN surface coverage) is more permeable for the passage of the redox probe toward the electrode surface.

3.2. *Electrochemical detection of thrombin using Si nanonet based aptasensors*

The formation of our Si NN-based aptasensor was optimized selecting the Si NN density of 54% with an aptamer concentration of 50 μM. It allows subsequent studies of the aptasensor characteristics, *i.e.,* sensitivity and specificity. Before, a study was carried out where the two surface densities of Si NN (*i.e.,* 15 and 54%) were subjected to a high concentration of thrombin (0.5 μmol L^{-1}) in such a way to obtain a high signal variation (data not shown). Steric hindrance due to thrombin recognition naturally induces a deceleration of the electron transfer rate, which results in an increase in charge transfer resistance. When both biosensors are incubated with 0.5 μmol L^{-1} of thrombin, R_{ct} increases by 540 Ω which corresponds to 20% of resistance before incubation for the biosensor containing 54% Si NN and it increases by 2400 Ω *i.e.* 35% for the biosensor containing 15% Si NN. So, the best response was obtained in the case of Si NN 15%. Thus, the most permeable modified electrode (Si NN 54%) for the redox probe was not the most sensitive toward thrombin. This seems to indicate that when the electron transfer of the redox probe is very fast (case of 54% without thrombin), the deceleration is less dramatic in the presence of thrombin, which leads to a lower sensitivity. For this reason, the studies presented hereafter were carried out on Si nanonet-based electrochemical aptasensors, presenting the characteristics that showed the best results: a Si nanonet covering 15% of the electrode surface and biofunctionalized using a 50 μmol L^{-1} TBA-15 bioreceptor solution.

3.2.1. *Sensitivity*

The Si NN-based aptasensors were then exposed to a given concentration of thrombin, in the range of 5 nmol.L^{-1} to 2 μmol L^{-1} in order to study its sensitivity. Fig. 5 presents the results of the sensitivity study obtained by cyclic voltammetry. The increase in thrombin concentration from 5 nmol.L^{-1} to 2 μmol L^{-1} (close to the thrombin solubility limit) implies a systematic decrease in the anodic current response, I_{pa} (Fig. 5A). Fig. 5B illustrates the I_{pa} obtained as a function of the logarithm of thrombin concentration. Based on the observed linearity in this

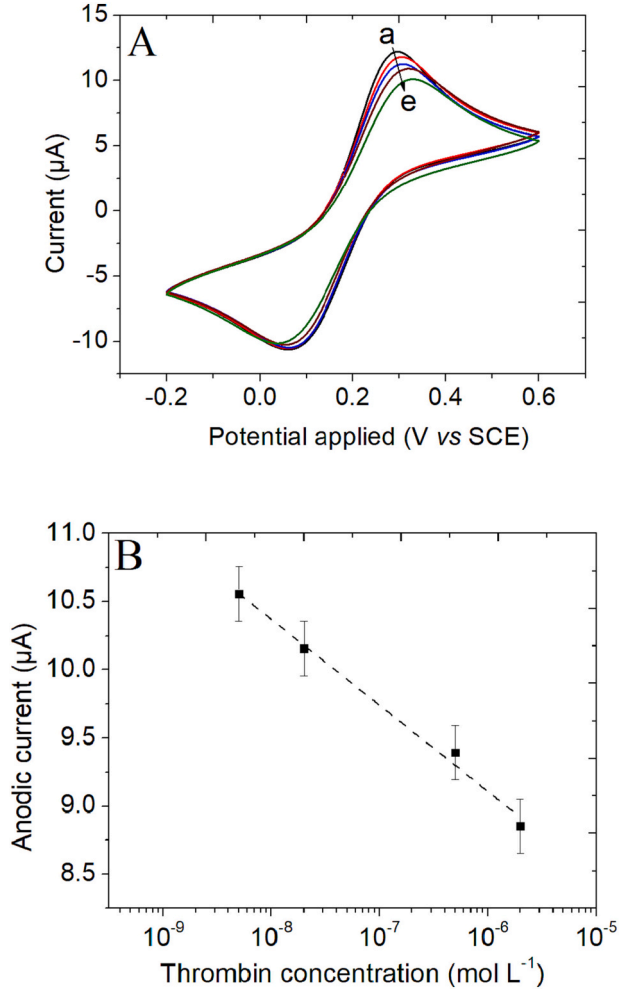

Fig. 5. (A) Cyclic voltammogram recorded at scan rate of 10 mV/s obtained for the GC/Si nanonet (15%)-based biosensor after incubation in different thrombin concentrations: (a) 0; (b) 5.10^{-9}; (c) 5.10^{-8}; (d) 5.10^{-7}; (e) 2.10^{-6} mol L^{-1}. Measurements performed using 22 mmol L^{-1} $[Fe(CN)_6]^{3-/4-}$ redox probe in 0.1 mol L^{-1} phosphate buffer (pH 7), at 25 °C. (B) Calibration curve for the thrombin biosensor corresponding to the changes in the anodic current peak (I_{pa}) upon detection of different thrombin concentrations. Experimental data (squares) and linear regression (line) are presented.

linear-log representation, the biosensor sensitivity can be defined as the slope of the curve, whose value corresponds to 0.63 ± 0.04 μA per order of magnitude, presenting a correlation coefficient $R^2 = 0.992$. These results evidenced that the recognition of the thrombin by the TBA-15 aptamer generated new steric hindrance to the redox probe diffusion toward electrode surface as the concentration of thrombin rose. In the EIS detection case, the range of concentrations studied was extended to the limit of thrombin solubility (2 μmol L^{-1}). The results obtained by EIS (Fig. 6) are in good agreement with those obtained by CV. In the Nyquist plot obtained, it is clearly evidenced that the radii of semicircle increased gradually with the thrombin concentration in a range from 5 nmol.L^{-1} to 0.5 μmol L^{-1}. Table 3 shows the obtained values after fitting the data to a standard Randles equivalent circuit.

All the studied parameters changed after thrombin recognition. It can be observed that the double-layer capacitance increased slightly with the thrombin concentration. The quasi-stability of C_{dl} may indicate that although the fixation of the protein on the TBA-15 bioreceptor generated a disturbance in the flow of $[Fe(CN)_6]^{3-/4-}$ redox species toward the electrode surface, the thrombin molecules had only a minor effect on the dielectric structure of the electrochemical interface. Finally, the results obtained for the characteristic frequency showed, as

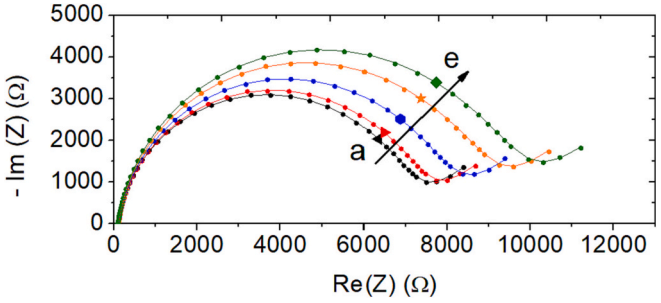

Fig. 6. Nyquist plot of impedance spectra obtained for the Si nanonet (15%)-based biosensor after incubation in different thrombin concentrations: (a) 0; (b) 5.10^{-9}; (c) 2.10^{-8}; (d) 5.10^{-8}; (e) 5.10^{-7} mol L^{-1} obtained at OCP, with an amplitude alternative potential of 10 mV_{RMS} and a frequency sweep from 50,000 Hz to 0.1 Hz. Dots represent the experimental data and lines represent the fitted data. The larger dots correspond to the frequency 3.46 Hz. Measurements performed using 2 mmol L^{-1} $[Fe(CN)_6]^{3-/4-}$ redox probe in 0.1 mol L^{-1} phosphate buffer (pH 7), at 25 °C.

Table 3
Values of the equivalent circuit elements obtained by data fitting for a Si nanonet-based electrochemical biosensor upon detection of different thrombin concentrations.

[Th] (mol L^{-1})	R_{ct} (Ω)	C_{dl}* (μF)	f (Hz)	$Z_{3.46\ Hz}$ (Ω)
0	6900 ± 100	1.8 ± 0.3	13.2	6667
5×10^{-9}	7100 ± 100	1.8 ± 0.3	12.3	6991
2×10^{-8}	7700 ± 100	1.8 ± 0.3	11.2	7310
5×10^{-8}	8600 ± 100	1.9 ± 0.3	9.8	7951
5×10^{-7}	9300 ± 100	1.9 ± 0.3	8.9	8469

* C_{dl} is calculated from the value of the CPE.

expected, that electron transfer is slowed. The steric hindrance generated by the presence of thrombin complexed by TBA-15 is reflected in the decrease of this parameter.

The values corresponding to the charge transfer resistance (R_{ct}) deduced from the modeling were plotted on a log-linear scale, as shown in Fig. 7 (A). One has to keep in mind that obtaining the Rct value is highly time-consuming and quite complicated to succeed. Indeed, standard EIS requires to record the impedance spectra over a wide frequency range, followed by the modeling process. For these reasons, we explore an alternative and simplified measurement protocol for the Si nanonet-based impedimetric biosensor. This interesting alternative consists in taking a single measurement at a given frequency. Herein, we measured the impedance modulus at 3.46 Hz. Indeed, this frequency value is located near the end of the semicircle, where the greatest impedance variations are observed after thrombin incubation. This approach would allow us to elaborate a calibration curve for the Si nanonet-based impedimetric biosensor in an easier and faster way. Then, $Z_{3.46\ Hz}$ was also plotted in the log-linear scale (Fig. 7 (B)), in order to validate the simplified protocol. For both measurement protocols, a linear correlation is obtained (Fig. 7) in the concentration range studied. The calibration curves obtained for these parameters presented a sensitivity of 1130 ± 180 Ω ($R^2 = 0.953$) and 770 ± 120 Ω ($R^2 = 0.953$) per order of magnitude, respectively. It can be noted that, as expected, the sensitivity is better when the charge transfer resistance (R_{ct}) is determined. However, measuring the impedance at a single frequency ($Z_{3.46\ Hz}$), which is easier to carry out, also provided very good sensitivity. By repeating the same studies (CV and EIS) on three different Si nanonet-based electrochemical biosensors, the repeatability of both devices and electrochemical techniques was evaluated. For each studied biosensor, similar results to those reported in this section were found over the same thrombin concentration ranges. As a conclusion, the Si nanonet-based aptasensors evaluated by both electrochemical techniques studied were able to detect thrombin from 5 nmol L^{-1} to the μmol

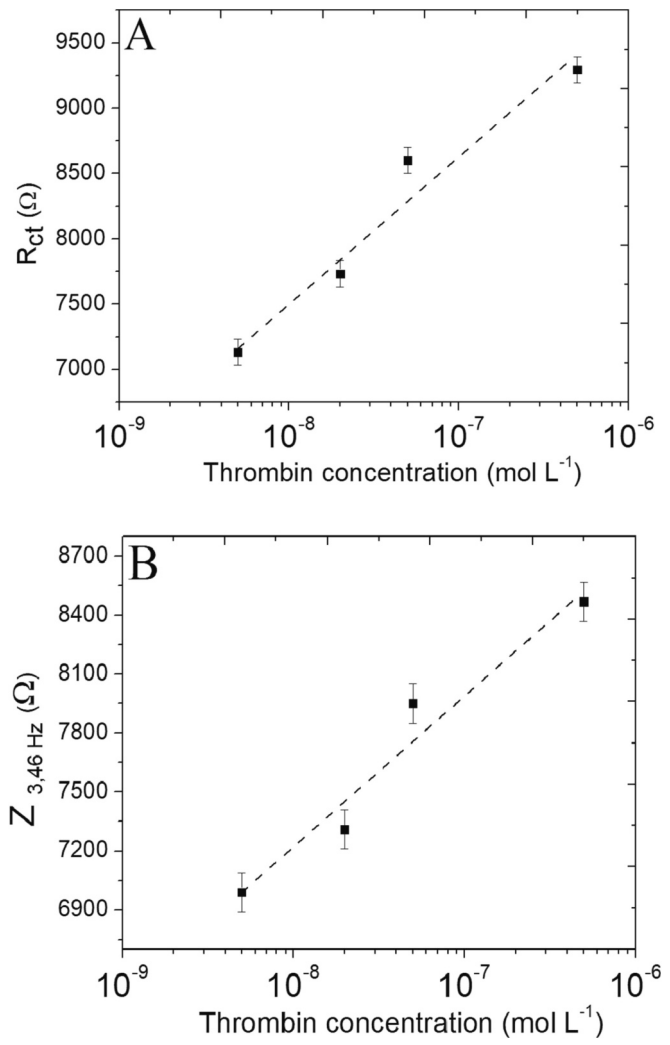

Fig. 7. Study of the different parameters obtained by EIS as a function of thrombin concentration: (A) charge transfer resistance, (B) impedance modulus at 3.46 Hz. Experimental data (squares) and linear regression (lines) are presented.

L^{-1} range, thus offering promising results for their use in the detection of thrombosis. Indeed, thrombin levels from 5 to 20 nmol L^{-1} in the blood indicate a high risk of thrombosis, while thrombin concentrations above 20 nmol L^{-1} already indicate the presence of thrombosis [58,59].

3.2.2. *Specificity*

To investigate the specificity of the Si NN-based aptasensors, control experiments were carried out. The devices biofunctionalized until the TBA-15 grafting step were incubated for 40 min in different aqueous protein solutions (0.5 μmol L^{-1}): lysozyme from hen egg white, Human immunoglobulin G (IgG) and bovine serum albumin (BSA). The determination of the possible non-specific adsorption of these proteins was evaluated by cyclic voltammetry and EIS. The results obtained were evaluated in terms of the relative variations of the anodic peak current (ΔI_{pa}) and the charge transfer resistance (ΔR_{ct}), with respect to the values obtained for the biosensor before exposure to the corresponding protein. These results, in turn, were compared with the values obtained for the detection of thrombin at the same concentration (Table 4).

As can be seen in Table 4, a decrease of 7% and 10% of the anodic peak is observed for lysozyme and human IgG associated with an increase of charge resistance transfer of 17% and 9%, respectively. Although the response of the Si NN-based aptasensors to these proteins appears relatively important, it is lower than the response obtained in the case of thrombin recognition, which presented a relative variation more important compared to the one obtained for lysozyme and IgG.

Table 4
Relative variations in the anodic peak current (ΔIpa), and the charge transfer resistance (ΔR_{CT}) for Si NN based biosensors exposed to different aqueous protein solutions (0.5 μmol L^{-1}).

	ΔI_{pa} (%)	ΔR_{ct} (%)
Thrombin	−18	+35
Lysozyme	−7	+17
Human IgG	−10	+9
BSA	+10	−19

In contrast, the behavior obtained was opposite in the case of BSA, with an increase of 10% in the anodic peak and a decrease of 19% in impedance (Table 4). The variation in the presence of thrombin remains higher but of the opposite sign. In the literature, it was found that at high BSA concentrations (above 800 nmol L^{-1}), non-specific interactions between TBA-15 and BSA can occur [59]. Thus, one hypothesis that could explain this result would be that the interaction between the TBA-15 bioreceptor and BSA may result in an aptamer unfolding that could favor the passage of the redox probe toward the electrode surface. This would mean, for example, that under this interaction, TBA-15 would present a more linear conformation instead of the G-quadruplex conformation necessary for thrombin recognition.

In addition, the difference observed with these three proteins is certainly linked to their isoelectric point, which are basic for lysozyme (10.5 to 11), quasi-neutral for IgG (6.6 to 7.2) and acid for BSA (5 to 5.5). The charges (positive or negative, in large or small quantities) provided by the proteins can lead to a modification of the conformation of the surface aptamer to adapt to this environment. For thrombin (7.0–7.6), lightly charged, with the relative variation being very significant, there is no doubt that the response is due to the recognition by the aptamer.

4. Conclusions

For the first time, we created Si NN-based aptasensors for electrochemical detection of thrombin. Meanwhile, we have shed light on the effect of Si NN surface density on the fabrication step. The Si NNs were successfully biofunctionalized after being mounted on a glassy carbon electrode *via* chemical polymerization of conductive polypyrrole-NTA, followed by TBA 15 bioreceptor grafting. The effectiveness of these processes was evaluated using SEM, EIS, and CV analyses. The Si NN serves as a support structure for the polypyrrole-NTA layer, resulting in a nanoporous structure on the GC electrode. The permeability for electron transport from the $[Fe(CN)_6]^{3-/4-}$ redox probe was increased as compared to a dense and continuous polypyrrole-NTA film with no nanonet (0% Si NN). This was especially evident in the case of Si NN's denser surface coverage (54%) toward lower surface density (15%). In contrast, thrombin electrochemical detection was carried out with the lowest density of Si NN (15%), resulting in less steric hindrance due to thrombin-aptamer interaction. Because of the low density, a superior recognition signal was obtained.

Good results were obtained for thrombin detection, as the aptasensor was capable of detecting thrombin in amounts regarded to be a marker of risk or presence of thrombosis. On the one hand, CV studies revealed a linear relationship between the measured current and the logarithm of the thrombin concentration ranging from 5 nmol L^{-1} to 2 μmol L^{-1}, with a sensitivity of 0.64 A per order of magnitude. Impedance measurements, on the other hand, revealed a linear relationship between the charge transfer resistance as well as the impedance modulus (at 3.46 Hz) and the logarithm of the thrombin concentration, with sensitivity of 1130 ± 180 Ω and 770 ± 120 Ω /log unit, respectively.

The specificity of the aptasensor may be tested using lysozyme, IgG, and BSA because the detection of thrombin causes a higher signal

variation than the disruption generated by the presence of one or both of its components. Further studies should focus on the effect of adjusting the morphological characteristics of Si NNs in order to increase the sensitivity and selectivity of Si NN-based electrochemical aptasensors. These promising results pave the way for exciting new projects involving the utilization of Si nanonet frameworks in electrochemical biosensing.

Declaration of Competing Interest

"There are no conflicts to declare".

Data availability

Data will be made available on request.

Acknowledgements

IRS-IDEX program of UGA (French National Research Agency in the framework of the "Investissements d'avenir" program, ANR-15-IDEX-02, Project APTANANOFET), NanoBio-ICMG platforms (UAR 2607), LabEx "Arcane" (ANR-11-LABX-0003-01) and CBH-EUR-GS (ANR-17-EURE-0003) are acknowledged for their support as well as Dr. Bassem Salem (LTM, Grenoble, France) for the Si nanowire growth.

References

[1] L. Xue, Z. Lyu, Y. Luan, X. Xiong, J. Pan, G. Chen, H. Chen, Polym. Chem. 6 (2015) 3708.
[2] K. Urmann, S. Arshavsky-Graham, J.G. Walter, T. Scheper, E. Segal, Analyst 141 (2016) 5432.
[3] H. Yu, O. Alkhamis, J. Canoura, Y. Liu, Y. Xiao, Angew. Chem. Int. Ed. 60 (2021) 16800.
[4] L. Li, S. Xu, H. Yan, X. Li, H.S. Yazd, X. Li, T. Huang, C. Cui, J. Jiang, W. Tan, Angew. Chem. Int. Ed. 60 (2021) 2221.
[5] K. Urmann, J. Modrejewski, T. Scheper, J.-G. Walter, BioNanoMat 18 (1–2) (2017) 20160012.
[6] H. Yoo, H. Jo, S. Soo Oh, Mater. Adv. 1 (2020) 2663.
[7] Q. Palomar, C. Gondran, M. Holzinger, R. Marks, S. Cosnier, Biosens. Bioelectron. 97 (2017) 177.
[8] H. Xu, K. Gorgy, C. Gondran, A. Le Goff, N. Spinelli, C. Lopez, E. Defrancq, S. Cosnier, Biosens. Bioelectron. 41 (2013) 90.
[9] A.V. Porfireva, G.A. Evtugyn, A. Ivanov, T. Hianik, Electroanalysis 22 (2010) 2187.
[10] M. Holzinger, A. Le Goff, S. Cosnier, Front. Chem. 2 (2014) 63.
[11] E. Morales-Narvaez, L. Baptista-Pires, A. Zamora-Galvez, A. Merkoci, Adv. Mater. 29 (2017) 1604905.
[12] Y.-L. Chen, C.-Y. Lee, H.-T. Chiu, J. Mater. Chem. *B* 1 (2013) 186.
[13] M. McMullan, N. Sun, P. Papakonstantinou, M. Li, W. Zhou, D. Mihailovic, Biosens. Bioelectron. 26 (2011) 1853.
[14] Q. Palomar, C. Gondran, J.-P. Lellouche, S. Cosnier, M. Holzinger, J. Mater. Chem. B 8 (2020) 3566.
[15] J. Ramanujam, D. Shiri, A. Verma, Mater. Express 1 (2011) 105.
[16] A. Zhang, J.-H. Lee, C.M. Lieber, Nano Today 38 (2021), 101135.
[17] L. Chen, X. Liu, B. Su, J. Li, L. Jiang, D. Han, S. Wang, Adv. Mater. 23 (2011) 4376.
[18] T. Arjmand, M. Legallais, T.T.T. Nguyen, P. Serre, M. Vallejo-Perez, F. Morisot, B. Salem, C. Ternon, Nanomaterials 12 (2022) 1043.
[19] Y. Zhao, G. Grüner, J. Mater. Chem. 22 (2012) 24983.
[20] P. Serre, C. Ternon, V. Stambouli, P. Periwal, T. Baron, Sensors Actuators B Chem. 182 (2013) 390.
[21] T.T.T. Nguyen, T. Cazimajou, M. Legallais, T. Arjmand, V.H. Nguyen, M. Mouis, B. Salem, E. Robin, C. Ternon, Nano Futur. 3 (2019), 025002.
[22] M. Vallejo-Perez, C. Ternon, N. Spinelli, F. Morisot, C. Theodorou, G. Jayakumar, P.-E. Hellström, M. Mouis, L. Rapenne, X. Mescot, B. Salem, V. Stambouli, Nanomaterials 10 (2020) 1842.
[23] J. Huang, Y. Zhu, H. Zhong, X. Yang, C. Li, A.C.S. Appl, Mater. Interfaces 6 (2014) 7055.
[24] B. Tao, J. Zhang, S. Hui, L. Wan, Sensors Actuators B Chem. 142 (2009) 298.
[25] L. Maiolo, D. Polese, A. Pecora, G. Fortunato, Y. Shacham-Diamand, A. Convertino, Adv. Healthc. Mater. 5 (2016) 575.
[26] Y. Liu, A. Rahimian, S. Krylyuk, T. Vu, B. Crulhas, G. Stybayeva, M. Imanbekova, D. S. Shin, A. Davydov, A. Revzin, ACS Sens. 2 (2017) 1644.
[27] Q. Yan, Z. Wang, J. Zhang, H. Peng, X. Chen, H. Hou, C. Liu, Electrochim. Acta 61 (2012) 148.
[28] J. Yin, X. Qi, L. Yang, G. Hao, J. Li, J. Zhong, Electrochim. Acta 56 (2011) 3884.
[29] S. Hui, J. Zhang, X. Chen, H. Xu, D. Ma, Y. Liu, B. Tao, Sensors Actuators B Chem. 155 (2011) 592.
[30] D.H. Kwon, H.H. An, H.S. Kim, J.H. Lee, S.H. Suh, Y.H. Kim, C.S. Yoon, Appl. Surf. Sci. 257 (2011) 4650.
[31] H. Shashaani, M. Faramarzpour, M. Hassanpour, N. Namdar, A. Alikhani, M. Abdolahad, Biosens. Bioelectron. 85 (2016) 363.
[32] S. Su, Y. He, M. Zhang, K. Yang, S. Song, X. Zhang, C. Fan, S.T. Lee, Appl. Phys. Lett. 93 (2008), 023113.
[33] K. Yang, H. Wang, K. Zou, X. Zhang, Nanotechnology 17 (2006) S276.
[34] B. Nasr, G. Chana, T.T. Lee, T. Nguyen, C. Abeyrathne, G.M. D'Abaco, M. Dottori, E. Skafidas, Small 11 (2015) 2862.
[35] N. Mintz-Hemed, T. Yoetz-Kopelman, A. Convertino, A. Freeman, Y. Shacham-Diamand, J. Electrochem. Soc. 164 (2017) B253.
[36] W. Chen, H. Yao, C.H. Tzang, J. Zhu, M. Yang, S.T. Lee, Appl. Phys. Lett. 88 (2006), 213104.
[37] J.I. Abdul Rashid, N.A. Yusof, J. Abdullah, U. Hashim, R. Hajian, J. Mater. Sci. 51 (2016) 1083.
[38] J. Baur, M. Holzinger, C. Gondran, S. Cosnier, Electrochem. Commun. 12 (2010) 1287.
[39] A.C. Figueiredo, C.C. Clement, S. Zakia, J. Gingold, M. Philipp, P.J. Pereira, PLoS One 7 (2012), e34354.
[40] Y. Wu, P. Yang, J. Am. Chem. Soc. 123 (2001) 3165.
[41] Y. Cui, L.J. Lauhon, M.S. Gudiksen, J. Wang, C.M. Lieber, Appl. Phys. Lett. 78 (2001) 2214.
[42] N. Haddour, J. Chauvin, C. Gondran, S. Cosnier, J. Am. Chem. Soc. 128 (2006) 9693.
[43] Y.M. Yasuo Kudoh, Kenji Akami, Synth. Met. 95 (1998) 191.
[44] J.J. Villora-Picó, V. Belda-Alcázar, M.J. García-Fernández, E. Serrano, A. Sepúlveda-Escribano, M.M. Pastor-Blas, Langmuir 35 (2019) 6089.
[45] Y. Perets, L. Matzui, L. Vovchenko, I. Ovsiienko, O. Yakovenko, O. Lazarenko, A. Zhuravkov, O. Brusylovets, Nanoscale Res. Lett. 11 (2016) 370.
[46] E. Pigois-Landureau, Y.F. Nicolau, M. Delamar, Synth. Met. 72 (1995) 111.
[47] C. Perruchot, M.M. Chehimi, M. Delamar, E. Cabet-Deliry, B. Miksa, S. Slomkowski, M.A. Khan, S.P. Armes, Colloid Polym. Sci. 278 (2000) 1139.
[48] P.O. Scokart, P.G. Rouxhet, J. Chem. Soc. Faraday Trans. 1 Phys. Chem. Condens. Phases. 76 (1980) 1476.
[49] A.D. Hiwarkar, V. Chandra Srivastava, I.D. Mall, RSC Adv. 4 (2014) 39732.
[50] M.E. Orazem, N. Pébère, B. Tribollet, J. Electrochem. Soc. 153 (2006) B129.
[51] T. Pajkossy, Solid State Ionics 176 (2005) 1997.
[52] N. Haddour, S. Cosnier, C. Gondran, J. Am. Chem. Soc. 127 (2005) 5752.
[53] L. Schmitt, C. Dietrich, R. Tampé, J. Am. Chem. Soc. 116 (1994) 8485.
[54] S.R. Hart, M.D. Waterfield, A.L. Burlingame, R. Cramer, J. Am. Soc. Mass Spectrom. 13 (2002) 1042.
[55] I. Kazane, K. Gorgy, C. Gondran, N. Spinelli, A. Zazoua, E. Defrancq, S. Cosnier, Anal. Chem. 88 (2016) 7268.
[56] J. Baur, C. Gondran, M. Holzinger, E. Defrancq, H. Perrot, S. Cosnier, Anal. Chem. 82 (2010) 1066.
[57] D. McCormick, L. Wright, H. Sigel, R. Griesser, B. Prijs, Biochemistry. 8 (1969) 2687.
[58] K.G. Mann, Circulation 124 (2) (2011) 12, p225.
[59] A. Trapaidze, J.P. Hérault, J.M. Herbert, A. Bancaud, A.M. Gué, Biosens. Bioelectron. 78 (2016) 58.